JOURNAL OF GEOPHYSICAL RESEARCH, VOL. 101, NO. C5, PAGES 12,097–12,110, MAY 15, 1996

Bar/trough generation on a natural beach

E. B. Thornton and R. T. Humiston[1]
Oceanography Department, Naval Postgraduate School, Monterey, California

W. Birkemeier
Field Research Facility, U.S. Army Corps of Engineers, Kitty Hawk, North Carolina

Abstract. Mechanisms for bar/trough generation are examined using velocities measured in the field applied to the *Bowen* [1980]/*Bailard* [1981] energetics-based sediment transport model. Measurements consist of a cross-shore array of nine electromagnetic current meters spanning the surf zone and daily bathymetric surveys during a 10-day period during which two storms occurred, when the bathymetry evolved from a three-dimensional terrace to a well-developed linear bar. The model predicts bed and suspended load transport separately based on various velocity moments. The velocities are partitioned into mean currents, low-frequency infragravity and shear instabilities (<0.05 Hz), and high-frequency short waves and turbulence (>0.05 Hz) to determine the relative importance of various mechanisms to the total transport. Velocity moments are computed over 90-min intervals to resolve tidal fluctuations. Tidal signatures were apparent in all modes of transport. Predicted transport rates are integrated and compared with daily cross-shore bathymetric profiles (averaged over a 400-m length of beach). The suspended load terms were an order of magnitude greater than bed load terms owing to the low fall velocity of the fine-grain sand within the surf zone. Model results for this experiment indicate the dominant mechanism for bar development was sediments mobilized by the strong longshore current and incident short waves within the surf zone and transported offshore by the mean undertow and shoreward transport onshore due to short wave velocity skewness. Using standard coefficients, the model correctly predicted the first-order movement of the bar during storms, but underpredicted trough development, and did not always perform well during mild wave conditions.

Introduction

A number of hypotheses have been proposed to explain bar generation. *Holman and Sallenger* [1993] reviewed bar generation mechanisms with specific discussion of earlier experiments at Duck, North Carolina, a barred beach and the site of the experiment described herein. The previous experiments found the bar system to be both spatially and temporally variable. During storms the bar can move rapidly offshore and become linear. With the cessation of the storm the bar rapidly returns to three-dimensional forms. It is generally thought that the incident wind waves are primarily responsible for mobilization of sediments, which can then be acted upon by a number of different transport mechanisms to form bars.

The two leading explanations for bar generation are the breakpoint mechanism and infragravity waves. *Dyhr-Nielsen and Sorensen* [1970] were the first to describe qualitatively the breakpoint bar model as a combination of undertow, explained due to radiation stress arguments, transporting mobilized sand offshore within the surf zone and converging with sand transported onshore due to the skewness of nonlinear waves just outside the surf zone to form a bar near the point of wave breaking. *Dally and Dean* [1984] model bar formation due to monochromatic waves generating an undertow, driving suspended sediment, and converging at the breakpoint. *Stive and Battjes* [1984] derived a similar model for random waves. *Stive* [1986] showed the importance of including wave asymmetry to explain shoreward transport. The main criticism of this mechanism for predicting bar location is that it does not appear to define a scale for bar location. The bar location scales as $H/\tan\beta$, where $\tan\beta$ is the beach slope; hence the breakpoint on planar beaches would be dependent on the incident wave height, which is variable in nature. However, if a bar previously exists, the breakpoint mechanism tends to reinforce the bar by modifying the breaking wave and cross-shore current field in a positive feedback manner [*Holman and Sallenger*, 1993].

A second popular explanation for bar formation has been narrowband infragravity waves (surf beat and edge waves). This mechanism is attractive because it predicts well-defined cross-shore bar scaling. At the location of nodes and antinodes, constructive velocity convergences occur at length scales comparable to observed bar locations. Further, they form a convenient explanation for why the spacing of multiple bars increases offshore as the spacing of nodes (antinodes) also increases offshore. This mechanism has been demonstrated in the laboratory for monochromatic standing waves [e.g., *Carter et al.*, 1973]. On the other hand, little support for the bar formation hypothesis was found in experiments by *Dally* [1987] using bichromatic waves to generate strong surf beat; the results of the experiments appeared to favor the breakpoint mechanism instead.

Field measurements of pressures and velocities show infra-

[1]Now at Naval Pacific Meteorology and Oceanography Center, Pearl Harbor, Hawaii.

Paper number 96JC00209.

gravity waves to be generally broadband [*Guza and Thornton*, 1985b]. *Roelvink* [1993] modeled profile changes due to random incident waves and broadband surf beat, and compared his model with comparable laboratory measurements; he concluded that cross-shore infragravity waves are not important to bar formation, although they can play an important destructive role in bar evolution.

On the other hand, *Howd et al.* [1992] showed that longshore currents modify the dispersion and velocity structure of the edge wave cross-shore velocity field, which can result in constructive bar formation, even for broadband edge waves. The location and movement of the bar prediction by this mechanism agreed at least qualitatively with the same field observations described in this paper.

Greenwood and Osborne [1991] summarized previous studies on barred beaches and present results from a cross-shore array of velocity measurements; they found onshore migration of the inner bar correlated well with the skewness of the velocity distribution and that infragravity oscillations were only significant close to the shoreline.

In this paper, bar formation is examined within the framework of an energetics-based sediment transport model applied to velocity field data. The model is based on the earlier work of *Bagnold* [1956], who put forth the idea that bed load transport rate of sediment grains in a fluid can be related to the energy expended on transporting the grains by the fluid flow. *Bagnold* [1963, 1966] extended this hypothesis to include the relationship between the interior flow and the suspended load transport rate. As the grains are at different heights in the water column for the two modes of transport, the forces acting on the grains are distinctly different. A mode dependent efficiency factor was introduced to account for this difference. *Bowen* [1980] and *Bailard* [1981] (hereinafter referred to as Bowen/Bailard) independently developed similar transport models for oceanic beaches based on the work of Bagnold. Bailard's model assumes that autosuspension is not allowed and expands terms in a Taylor series, retaining only the first two terms to obtain a convenient form for analysis, which will be used here. The model predicts the total (i.e., bed and suspended load) alongshore and cross-shore transport rates over an arbitrary bottom topography.

There have been several previous applications of the Bowen/Bailard model to both field and laboratory data. *Richmond and Sallenger* [1984] examined sediment texture change at the Duck beach during a time when the sediments were poorly sorted (bimodal or broad distributions) and applied the model to various size fractions using velocity measurements from current meters mounted on a movable sled. They found course sediments may move shoreward due to wave velocity skewness while fine material may simultaneously move offshore due to undertow, resulting in sorting of the sediments; however, their preliminary analysis gave inconsistent prediction of transport. *Guza and Thornton* [1985a] applied Bailard's model to data acquired on the near planar, Torrey Pines Beach, California, and found that mean flow and low-frequency infragravity waves must be included to properly describe the velocity field for predicting sediment transport. *Roelvink and Stive* [1989] modeled the velocity terms in Bailard's model calculating random wave heights using *Battjes and Janssen* [1978] and applying nonlinear stream function theory locally [*Rienecker and Fenton*, 1981] to calculate velocities; they compared modeled results with two-dimensional laboratory measurements and found the short wave velocity skewness, undertow, and phase coupling of short wave velocity variance with long waves all to be significant contributors to the transport. Roelvink and Stive found that the model reasonably predicted the measured barred bathymetry using standard coefficients, but they had to multiply the total flow-induced transport by a factor of 2.

The objectives of this paper are to examine bar/trough generation mechanisms and to evaluate the ability of the Bowen/Bailard model to predict sediment transport from velocity measurements. The data were acquired during the nearshore processes experiment DELILAH conducted at Duck, North Carolina, and are composed of nine closely spaced velocity measurements extending from the shoreline to approximately 4.5 m depth. The data are unique in that they were continuously recorded over a period of 3 weeks, allowing examination of tidal effects. During the experiment the profile evolved from a terrace bar configuration to a well-developed linear bar. Since sediment transport was not measured directly, verification is by comparing predicted bathymetric changes to observed changes. The analysis is limited to examining the cross-shore transport only.

Model

In the following, bottom contours are assumed to be straight and parallel and the alongshore sediment transport rate q_y homogenous alongshore such that $\partial q_y/\partial y = 0$. Conservation of mass simplifies to

$$\frac{\partial q_x}{\partial x} = \mu \frac{\partial h}{\partial t} \tag{1}$$

where $\mu = 0.7$ is introduced to account for packing of the loose grains in the bed and h is depth. Equation (1) is used to calculate changes in bathymetry based on predictions of cross-shore sediment flux.

The time-averaged cross-shore sediment flux, expressed as volume sediment transport per unit width per unit time, is given by [*Bailard*, 1981]

$$\begin{aligned}\langle q_x(t)\rangle = {} & K_b(\langle|\mathbf{u}(t)|^2\tilde{u}(t)\rangle + \langle|\mathbf{u}(t)|^2\bar{u}\rangle) - K_{bg}\langle|\mathbf{u}(t)|^3\rangle \\ & + K_s(\langle|\mathbf{u}(t)|^3\tilde{u}(t)\rangle + \langle|\mathbf{u}(t)|^3\bar{u}\rangle) - K_{sg}\langle|\mathbf{u}(t)|^5\rangle\end{aligned} \tag{2}$$

where b, s, and g refer to bed load, suspended, and gravity, and

$$|\mathbf{u}(t)| = [\tilde{u}^2 + \tilde{v}^2 + \bar{u}^2 + \bar{v}^2 + 2(\tilde{u}\bar{u} + \tilde{v}\bar{v})]^{1/2} \tag{3}$$

is measured at the top of the bottom boundary layer. The overbar indicates mean velocity, and the tilde indicates oscillatory velocity. The coefficients are given by

$$K_b = \frac{\rho}{(\rho_s - \rho)g} C_f \frac{\varepsilon_b}{\tan\phi}$$

$$K_{bg} = K_b \frac{\tan\beta}{\tan\phi}$$

$$K_s = \frac{\rho}{(\rho_s - \rho)g} C_f \frac{\varepsilon_s}{W}$$

$$K_{sg} = K_s \frac{\varepsilon_s}{W} \tan\beta$$

where ρ is the water density, ρ_s is the density of quartz sand, C_f is the bed drag coefficient, ϕ is the internal friction angle of the

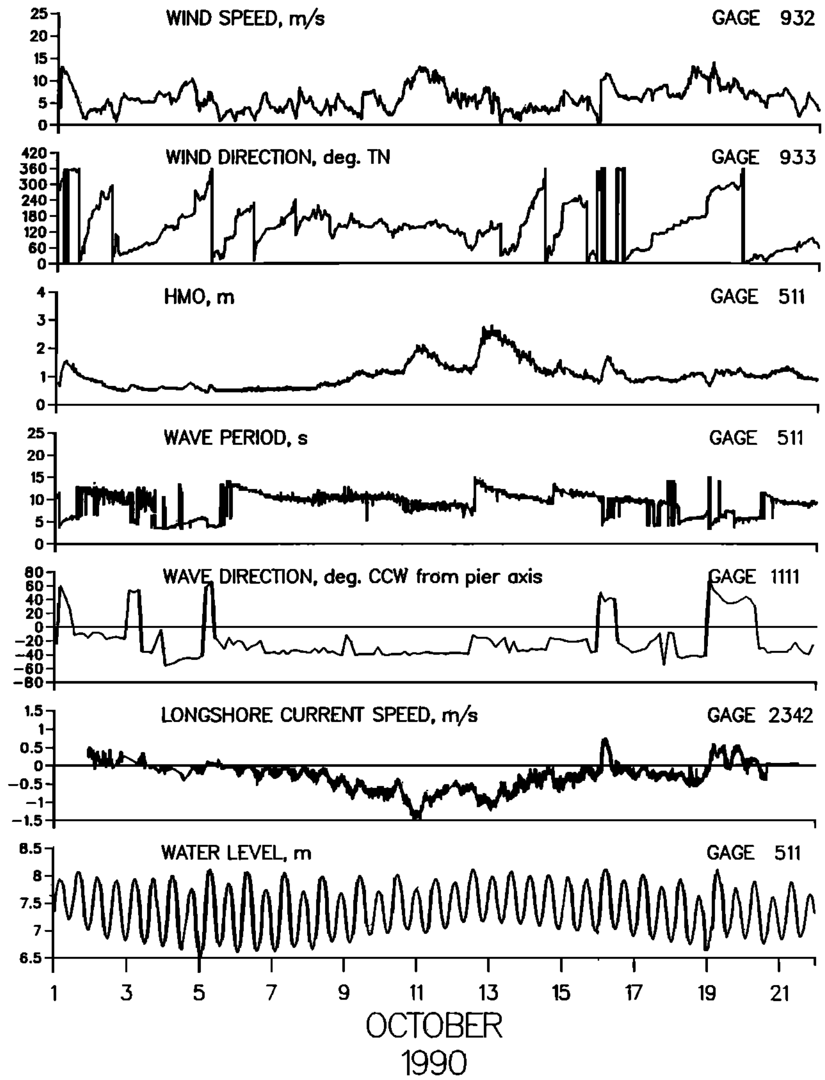

Figure 1. Environmental conditions during DELILAH.

grains in the bed, $\tan\beta$ is the local bed slope, and W is the fall velocity. The suspended and bed load efficiency factors, ε_s and ε_b, are the ratio of stream power to suspended and bed load work rates. The transport is positive in the offshore direction. The first three terms on the right-hand side of (2) represent the bed load contribution to total sediment transport, and the fourth through sixth terms represent the suspended load contribution. The third and sixth terms are the downslope transport contributions by gravity.

To examine various transporting mechanisms, the oscillatory terms ($\tilde{u}$, $\tilde{v}$) are further partitioned into low-frequency $\tilde{u}_l$ ($f < 0.05$ Hz) and high-frequency $\tilde{u}_s$ ($f > 0.05$ Hz) contributions such that

$$\mathbf{u}(t) = (\bar{u} + \tilde{u}_l + \tilde{u}_s)\hat{\imath} + (\bar{v} + \tilde{v}_l + \tilde{v}_s)\hat{\jmath} \tag{4}$$

The low-frequency velocities are primarily due to long waves and shear instabilities and henceforth are referred to as long waves. The high-frequency velocities are primarily due to short waves and turbulence and henceforth are referred to as short waves, but keep in mind, they include turbulent contributions which can be important, especially under breaking waves.

DELILAH Experiment and Velocity Measurements

Experiment

Data were acquired as part of the DELILAH nearshore processes experiment held at the Coastal Engineering Research Center, U.S. Army Engineer Waterways Experiment Station's Field Research Facility (FRF) in Duck, North Carolina, during October 1990. The period investigated is October 6–16. The environmental conditions are shown in Figure 1. Two storms occurred between October 9 and 13, during which time the significant wave height H_s increased and longshore currents $\bar{v}$ were strong. On October 9 a frontal system from the south arrived, resulting on October 10 in broadband waves with H_s up to 2 m incident at relatively large angles (about 40° from the south in 8 m depth), driving strong northward longshore currents ($\bar{v} \approx 1.5$ m/s). On October 13, narrowband swell ($H_s = 2.5$ m) arrived from the south due to distant hurricane Lili. Although these waves were larger than those on October 10, the incident wave angles were less (about 20° in 8

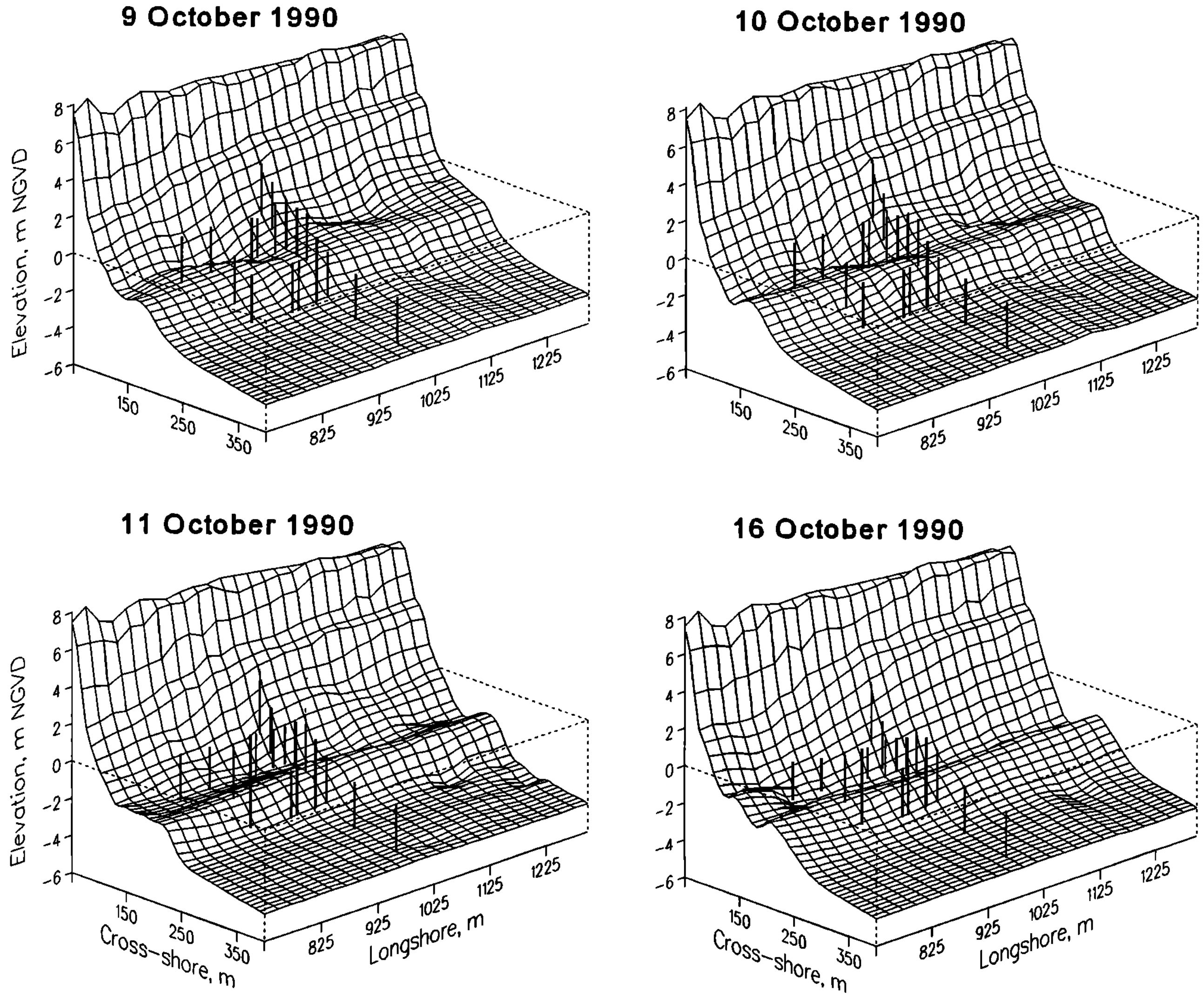

Figure 2. Bathymetry on October 9, 10, 11, and 16. Vertical lines indicate current meter locations.

m depth at the peak of the storm), and the resulting longshore currents were not as large ($\bar{v} \approx 1$ m/s).

The bathymetry was surveyed daily using the Coastal Research Amphibious Buggy (CRAB). The bathymetry up to October 9 shows significant variability in both the alongshore and cross-shore directions (Figure 2). After commencement of the storms the alongshore variability started to smooth out on October 10, and by October 11 most of the alongshore variation had vanished, and a linear longshore bar existed past October 16. Cross-shore profiles (Figure 3) were averaged alongshore between 200 m north and 200 m south of the current meter array to minimize the effect of longshore inhomogeneity.

The velocity data were obtained from a cross-shore array of nine Marsh McBirney, electromagnetic, bidirectional current meters located at about 975 m alongshore (see Figure 2). The velocity measurements were sampled at 8 Hz. The current meter locations (referred to as cm1–cm9 with distances offshore given in Table 1), and elevations (relative to National Geodetic Vertical Datum (NGVD)) are shown in Figure 3 (mean sea level is +0.01 NGVD). Data from a tide gage (located well outside the surf zone near the 5-m depth contour) were used to calculate the mean water level relative to NGVD. Velocity component data were numerically rotated to orient axes parallel and perpendicular to depth contours. Proper orientation is important to accurately resolve cross-shore velocities to avoid contamination by longshore currents. To be consistent with the model assumption of straight and parallel contours, beach orientation was determined for each day based on the direction of the 2-m contour averaged over 400 m alongshore (rotations as applied to all current meters for each day are given in Table 2). Measured currents appeared homogeneous alongshore, and no rip currents were observed during the experiment within the measurement area either visually or by the current meters, which included alongshore current meter arrays of five sensors in the trough and four sensors on the backside of the bar (locations are indicated as vertical lines in Figure 2).

The velocities were partitioned into low- and high-frequency time series using a Fourier filter. Typical velocity energy density spectra at locations cm2, 5, and 9 are shown in Figure 4. The velocities outside the surf zone at cm9 in ~4 m depth are predominantly due to shoaling, narrowband waves (peak frequency at 0.07 Hz), which exhibit nonlinear characteristics, resulting in a strong harmonic at 0.014 Hz. The velocities at cm5 are associated with waves breaking on the bar, resulting in

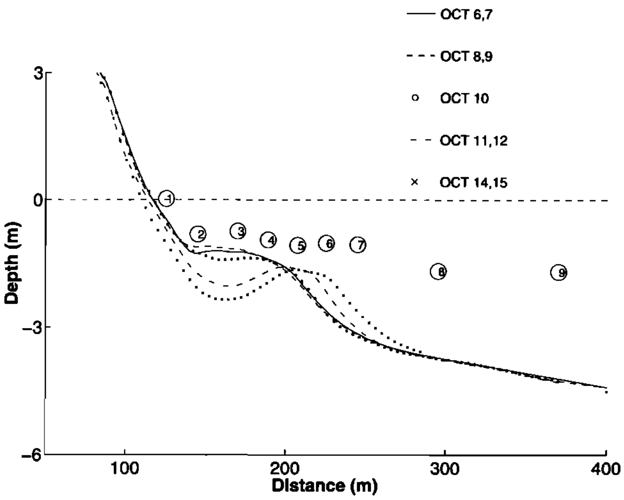

Figure 3. Bottom profiles (averaged over 400 m alongshore) during the experiment, with cross-shore current meter array elevations and locations indicated. Depths are relative to National Geodetic Vertical Datum, and cross-shore distances are in the U.S. Army's Engineer Waterways Experiment Station's Field Research Facility coordinates.

a decrease of the higher-frequency harmonic energy; low-frequency energy is increased in the form of infragravity and shear instabilities of the longshore current. At cm2 the energy at the long waves is comparable to the short waves. The low-frequency energy of cm5 and cm2 has considerable structure, consistent with nodes and antinodes of standing infragravity waves. As the frequencies of nodes and antinodes in the infragravity band are a function of the cross-shore distance, the spectra appear broadband across the infragravity portion of the spectrum. A spectral valley occurs at about 0.05 Hz, which makes it a logical frequency to partition the data into long and short waves. Complex Fourier transforms were calculated for the velocity time series, and inverse transforms were performed over only the low-frequency (0–0.05 Hz) or high-frequency (0.05–4.0 Hz) bands to obtain the two filtered time series. At the time of filtering the high-frequency band velocities were depth corrected down to the top of the bottom boundary layer (corresponding to velocity elevation in *Bailard's* [1981] model) using the linear wave theory transfer function applied to the complex spectral amplitudes

$$H(f) = \frac{1}{\cosh k(h + z_m)} \tag{5}$$

where k is the wave number and z_m is the current measurement elevation.

Quality assessment of the data determined that not all current meters functioned throughout the experiment. Data from cm1 was not used from October 6 to 10 as the sensor was frequently out of the water. Sections of current meters 3, 4, and 7 were noisy from October 10 to 14 and had to be edited and/or sections deleted; this resulted in some of the moments being averaged over records shorter than 90 min. At about 0700 LT on October 11, cm6 was lost; thereafter, bathymetry predictions are averaged between cm5 and cm7.

Sediment samples were collected on October 15 along a single profile line. No other sediment samples were taken. The samples were generally typical of sediments previously collected by the FRF over many years, with a wide range of coarse sediment size on the beach and foreshore and fine, well-sorted sand seaward (Table 1). The location of the shoreline at mean sea level was at an average cross-shore distance of 114 m relative to the FRF coordinates. Shoreward of cm1 (located at 125 m), sediment ranged in size from about 0.4 to 1.0 mm. Between cm2 (located at 145 m) seaward to cm9 (370 m) the mean grain size ranged from 0.12 to 0.2 mm. The standard deviations of the sediment distributions calculated using the method of moments show the sand is well sorted within the surf zone, with a much broader distribution on the foreshore.

Table 1. Sediment Mean Grain Size and Standard Deviations in a Cross-Shore Transect on October 15, 1990

Cross-Shore Distance,* m	Current Meter	Mean Grain Diameter, mm	Standard Deviation, mm
117		0.36	0.60
124		0.43	0.53
125	cm1		
138		0.12	0.76
145	cm2		
149		0.18	0.57
170	cm3		
189	cm4		
192		0.20	0.72
207	cm5		
226	cm6		
245	cm7		
256		0.14	0.70
295	cm8		
328		0.14	0.67
370	cm9		
484		0.16	0.69

*Distances are referenced to the Field Research Facility coordinates; approximate shoreline at mean sea level is located at 114 m.

Table 2. Daily Bathymetry Rotation Angles

Date in October	Angle, deg
6	2.8
7	3.2
8	3.0
9	4.4
10	4.0
11	2.5
12	2.6
13	2.5
14	1.1
15	2.5
16	2.4

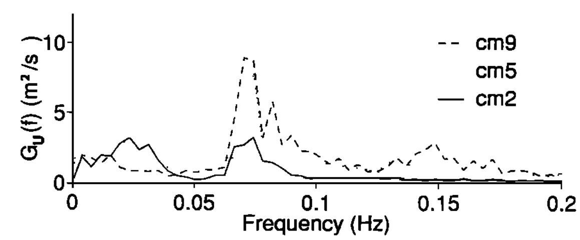

Figure 4. Kinetic energy spectra for the cross-shore velocity component at locations cm2 (solid line), cm5 (dotted line), and cm9 (dashed line) on October 12, 1990.

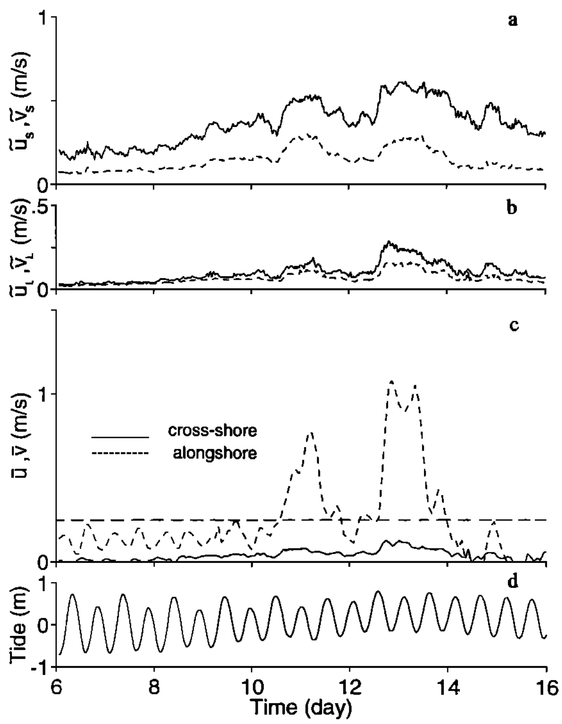

Figure 5. Time series of 90-min averages of cross-shore (solid line) and alongshore (dashed line) velocity standard deviations of (a) short wave components, (b) long wave components, (c) mean currents (dashed horizontal line is the threshold velocity for suspended sediments due to mean current), and (d) tide elevations at cm8 outside the surf zone.

In the application of the model an averaged mean grain size of 0.16 mm is used within the surf zone at locations cm2–cm9 and a grain size of 0.4 is used at location cm1.

Velocity Observations

Insight into the role of the velocity component contributions to sediment transport is obtained by examining velocity time series partitioned into mean current and standard deviations of long and short wave contributions for locations characteristic of the offshore (cm8), over the bar (cm5), and the inner surf zone (cm2) shown in Figures 5–7, respectively. During the storm periods the mean, short, and long wave velocity standard deviations were the same order of magnitude. The largest velocity contribution with the greatest variability was from the mean longshore current. At the peak of the storms the mean current exceeded 1 m/s at all three locations, and it dominates the modulus of the total velocity vector (equation (3)). The mean cross-shore current varied in magnitude across the surf zone and was always directed offshore in the form of an undertow.

The cross-shore short wave velocities were always greater than their alongshore values due to incident wave angles being less than 45°. The short and long wave contributions were of the same order inside the surf zone. Outside the surf zone, the short waves were always larger than the long wave contribution.

A definite tidal signature is evident in the velocities inside the bar, even though the mean tide range is relatively small (~1 m). *Thornton and Kim* [1993] show that the breaking wave heights are modulated by the time-varying depth of the tide and that the waves inside the barred profile are dependent on the breaking wave conditions over the bar. In general, short wave velocities have a strong tidal signature inside the surf zone. Since longshore currents are a function of radiation stress gradients associated with short wave breaking, $\bar{v}$ also has a strong tidal signature. *Thornton and Kim* [1993] present a simple model examining the relationships between the tide, wave heights, and longshore currents. On a planar beach with stationary wave conditions, the effect of the tide is to simply displace a constant longshore current distribution on and offshore, resulting in $\bar{v}$ being in phase with the tide in the inner surf zone and out of phase in the outer surf zone. A similar relationship occurs for a barred beach. Outside the surf zone, tidally driven currents can exist which have a different phase relation with the tidal elevation. The wave heights inside the surf zone are dependent on the breaking wave height over the bar, which is always in phase with the tide; therefore short wave velocity variances are in phase at all location across the surf zone.

Long waves are composed of infragravity surf beat (standing long waves reflected off the beach face), edge waves (long waves trapped to the shoreline), and shear instabilities of the longshore current. *Guza and Thornton* [1985b] and others have shown that infragravity energy within the surf zone is proportional to the offshore wave height. Therefore infragravity energy would be expected to more closely follow the offshore wave conditions than the short waves inside the surf zone and not exhibit a strong tidal signature. On the other hand, *Oltman-Shay et al.* [1989] showed that the magnitude of the shear instabilities are proportional to the strength of the longshore current. Since shear instabilities are proportional to the longshore current magnitude, they would be expected to be modulated by the tide and have the same phase relationships with the tide as the longshore current.

Examining the velocities partitioned into mean, short, and long wave contributions and starting outside the surf zone at cm8 (Figure 5), longshore and cross-shore mean currents and long wave velocities are all proportional to the incident short waves. Tidal signatures are most evident in the longshore current early in the experiment (October 6–10), when cm8 was well outside the surf zone, which is due to tidal currents [*Thornton and Kim*, 1993].

Over the bar at cm5 (Figure 6) the longshore current is the strongest velocity component and is strongly modulated and 180° out of phase with the tide (particularly evident during nonstorm periods). The undertow is stronger over the bar than in the trough (Figure 7) or offshore (Figure 5). The short wave velocities did not vary during the time of the experiment because of the saturated wave heights over the bar. During nonstorm periods of this experiment the long waves show a tidal signature which is out of phase with the tide and in phase with the longshore current, suggesting that shear instabilities may be important. On the other hand, during storms, infragravity waves are more energetic but lack a tidal signature, suggesting that surf beat and edge waves may be important.

In the inner surf zone (cm2; see Figure 7) the longshore current again makes the largest velocity contribution and is in phase with the tide. The short wave velocities at cm2 slowly increase due to an increase in water depth as the beach eroded (unlike cm5 and cm8, where the depth remained near constant; see Figure 3) and are in phase with the tide owing to energy saturation over the bar.

Cross-shore distributions of velocities for a time represen-

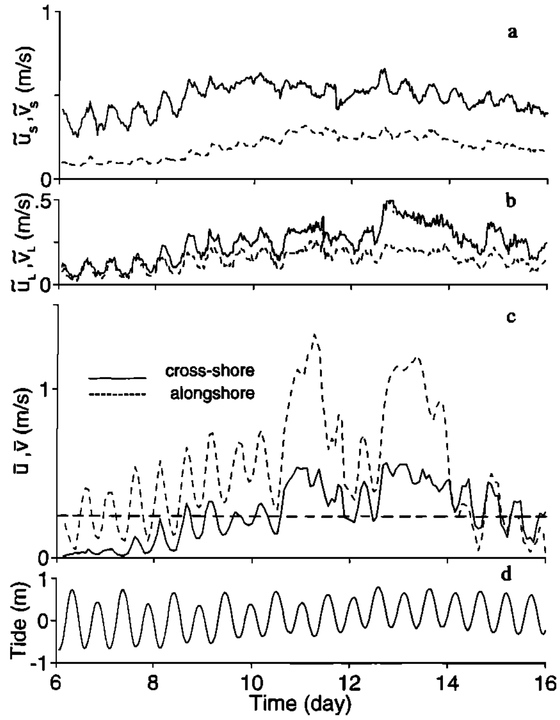

Figure 6. Same as Figure 5, except at cm5 over the bar.

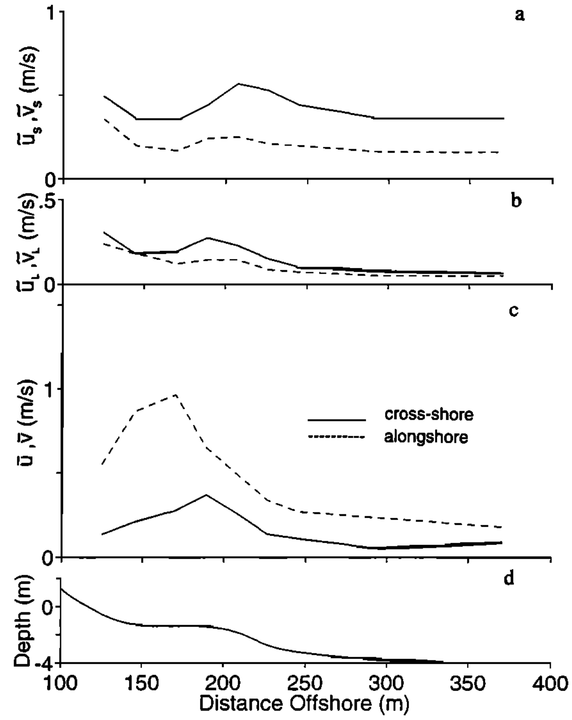

Figure 8. Cross-shore distributions of 90-min averages of cross-shore (solid line) and alongshore (dashed line) velocity standard deviations of (a) short wave components, (b) long wave components, (c) mean currents, and (d) bottom profile on October 10, 1990, at high tide.

tative at the start of the storms on October 10 at high tide are shown in Figure 8. The short waves increased in magnitude due to shoaling (indicated by the short wave rms velocities), broke on the bar, and reformed inside the surf zone; they again shoaled in the inner surf zone and broke on the foreshore. The longshore current is largely confined inside the bar on October 10, with a maximum in the trough.

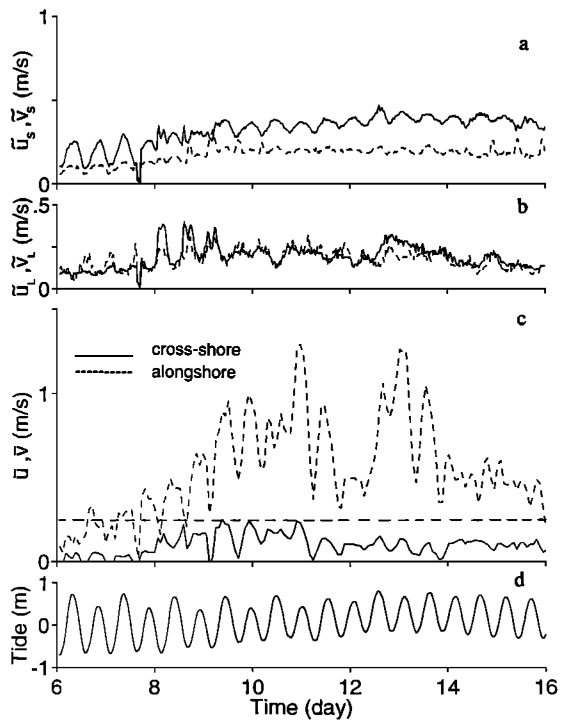

Figure 7. Same as Figure 5, except at cm2 in the inner surf zone.

Representative cross-shore distributions of velocities due to larger waves on October 12 at low tide are shown in Figure 9. The waves broke outside the bar, but they show a similar pattern inside the bar as on the October 10. The longshore current has a maximum over the trough but extends well offshore because of the spatial extent of wave breaking. In both cases the undertow show a maximum over the bar and a minimum in the trough. The long waves generally increase shoreward, with maxima over the bar and on the foreshore.

Application of Model

In the application of the Bowen/Bailard model to field data, standard coefficient values are used and no attempt is made to tune the model to the data. The efficiency factors ε_s and ε_b and the fall velocity W are specified based on mean grain size. The fall velocity for quartz grains of mean size 0.16 mm is 1.3 cm/s within the surf zone and for mean size 0.4 mm is 5 cm/s on the foreshore [*Komar and Reimers*, 1978]. On the basis of the internal friction angle for sand grains, $\tan\phi = 0.63$. A nominal value for $\varepsilon_s = 0.015$ is used after *Bagnold* [1966] and others [e.g., *Bowen*, 1980; *Bailard*, 1981]. *Bagnold* [1966] presents a functional relationship for ε_b with stream velocity and grain size. Using the mean grain size range of 0.12–0.2 mm found at Duck and velocity range of 1–2 m/s, $\varepsilon_b = 0.135 \pm 0.004$, indicating ε_b is insensitive to the observed conditions within the surf zone. A value of $\varepsilon_b = 0.125$ is used at location cm1, reflecting the larger mean grain size on the foreshore. A value of $C_f = 0.003$ was used, consistent with the value obtained

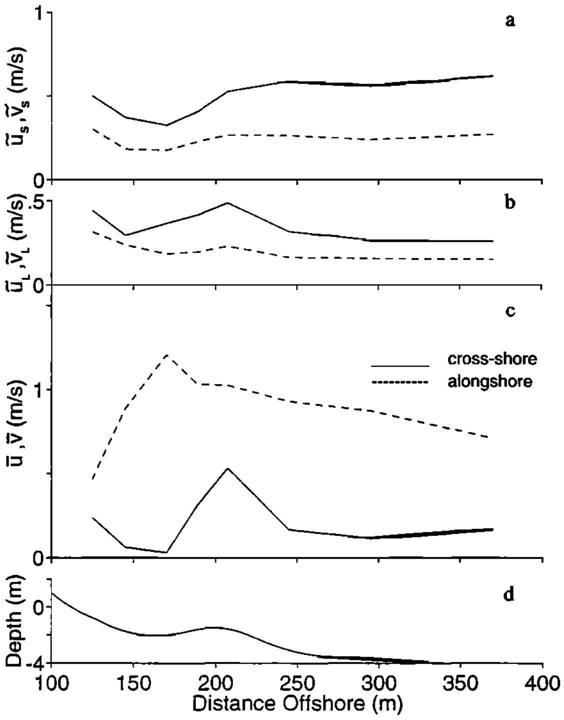

Figure 9. Same as Figure 8, except on October 12, 1990, at low tide.

from longshore current modeling of the DELILAH data [*Church and Thornton*, 1993]. The bottom slopes, tanβ, were calculated from the measured depths about each current meter for each day.

The sediment transport rates were partitioned into the six terms of (2) for bed and suspended load components. The downslope components of the bed and suspended load contributions (third and sixth terms of (2)) were generally smaller compared with the other terms. Time series of 90-min averages of the other four terms at cm2, 5, and 8, indicative of inner surf zone, over the bar, and offshore, are shown in Figure 10. Negative transport indicates onshore transport, and positive transport indicates offshore transport. In general, at all three locations the predicted suspended load is much larger than the bed load owing to the low fall velocity of the fine-grained sand. Fluctuations in transport are roughly of the same period as the tide, although magnitude and phase vary with time and location.

At cm8, onshore suspended transport owing to short wave skewness is opposed by offshore suspended transport due to undertow, with a net onshore transport. Both these mechanisms are associated with the short waves whose magnitude is governed by offshore conditions.

Over the bar at cm5 the transport is predominantly offshore due to transport by the undertow. During the milder wave conditions and before the bar was built (October 6–9), cm5 was generally outside the surf zone and shoaling short waves tended to move sand onshore due to wave asymmetry. Once the bar was established after October 10, the short waves broke on the bar. In the process of breaking on the bar, the short waves lose their skewness, becoming more Gaussian [*Guza and Thornton*, 1985a]; during the storms the model indicates offshore transport by the waves, which presumably is due to bound long waves. A tidal signature is evident in the transport terms due to the tide modulating the depth at which the waves break.

After passing over the bar, the waves reform and again shoal as they pass cm2. The waves become nonlinear as they shoal and again preferentially transport sand onshore due to their increased skewness. The onshore transport by the short waves is balanced primarily by offshore transport of the undertow, resulting in a net transport offshore during most of the experiment to build the bar. The short wave velocities at cm2 are indicative of waves in the inner surf zone whose amplitudes are primarily governed by depth of breaking over the bar. Hence the magnitudes of the transport terms do not strongly reflect the storms and tend to be more uniform over the 10-day period.

Predicted profile changes Δh between current meter positions are calculated using (1) and (2)

$$\Delta h = \frac{\Delta t}{\mu \Delta x} \sum_t \left[q(x_i, t) - q(x_{i+1}, t) \right] \tag{6}$$

where the sediment fluxes (calculated every 90 min) are integrated (summed) over Δt, the time between profile transects (nominally 24 hours), and $\Delta x = x_{i+1} - x_i$, the distance between current meters. The vertical lines in Figure 10 indicate when the profiles were measured at the cross-shore instrument array used in the Δh calculations.

Model results (equation (6)) of both profile and rate of

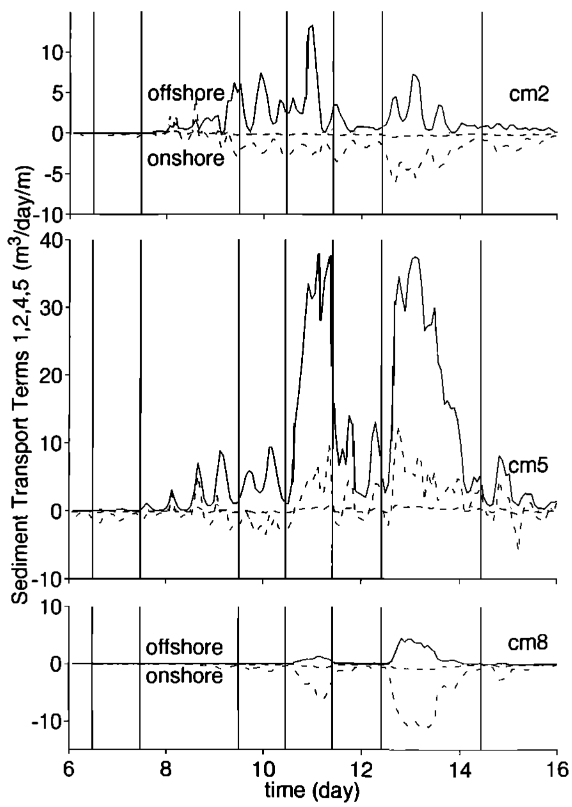

Figure 10. Time series of 90-minute averages of cross-shore components of immersed weight sediment transport per unit width at cm2, 5, and 8 for bedload terms $K_b\langle|\mathbf{u}|^2\bar{u}\rangle$ (dashed lines) and $K_b\langle|\mathbf{u}|^2\tilde{u}\rangle$ (dotted lines) and suspended sediment transport terms $K_s\langle|\mathbf{u}|^3\bar{u}\rangle$ (dash-dotted lines) and $K_s\langle|\mathbf{u}|^3\tilde{u}\rangle$ (solid lines) in (2). Positive is directed offshore. Vertical lines are times of bathymetry profiles.

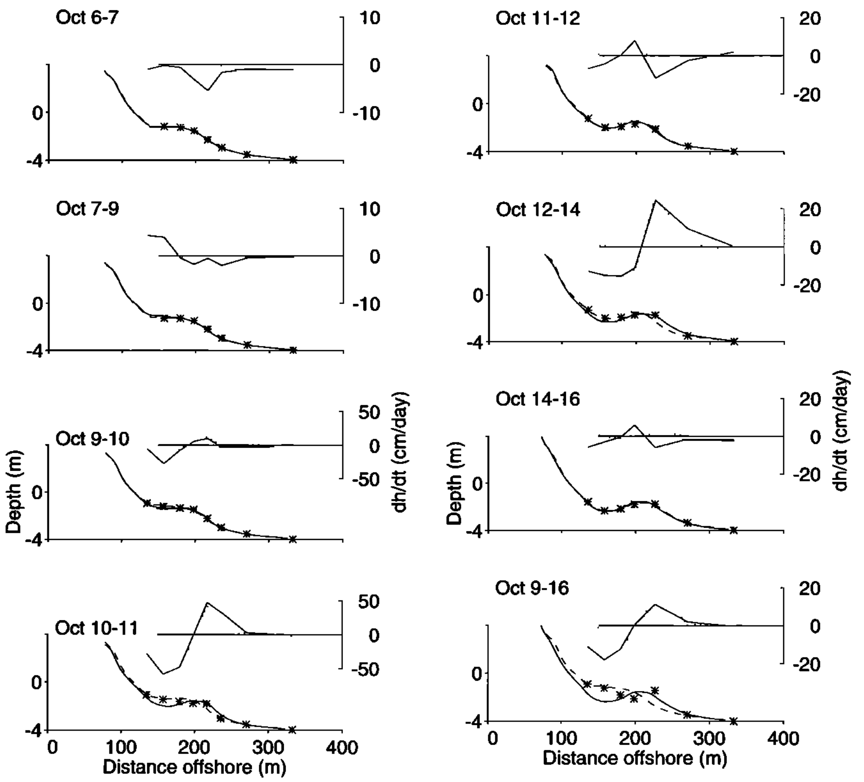

Figure 11. Predicted changes in bathymetry (left ordinate) and rate of change of bathymetry (right ordinate). Initial bathymetry (dashed lines) and measured bathymetry (solid lines) are compared with predicted (stars). The measured rate of change, dh/dt (solid lines), is compared with $(1/\mu\Delta x)\ \Sigma\ q(t)$, the predicted rate of change (dotted lines).

profile changes are compared with the observed bathymetry (Figure 11). The model qualitatively predicts the profile evolution. Day-to-day and cumulative changes are shown. Results for October 7–9 and 14–16 are combined as the changes are similar. October 12–14 is combined as there was no profile measured on the 13th.

There is little discernable difference between predicted and observed depths from October 6–9. With the onset of storm waves, October 9–10, a trough started to form between cm2 and cm3. Between October 10 and 11 the trough continued to develop and the bar migrated seaward. The model underpredicts the trough development on these days. During the decreased wave activity on October 11 and 12 there is little change in bathymetry, also reflected by the model. From October 12–14 the trough deepens and the bar migrates farther seaward. The model qualitatively predicts bar growth. As the waves subside, both the observations and model show little change. The cumulative change for the 10 days shows the model predicts the offshore movement of a bar with the bar displaced slightly offshore and underpredicts trough development.

A more sensitive diagnostic test of the model is a comparison of predicted and measured bathymetric changes (also shown in Figure 11; note different scales). The model correctly predicts onshore movement of sand from the offshore October 6–7, although underpredicted. The model correctly predicts growth and offshore bar migration during October 9–10, 10–11, and 12–14, which coincided with larger storm waves (see Figure 10), but it underpredicts trough development. However, during the milder wave conditions, when the changes were small (October 7–9, 11–12, and 14–16), the model also predicted offshore bar migration when, in fact, the bar was moving onshore. The predicted average rate of change October 9–16 slightly overpredicts the growth over the bar but underpredicts the trough development. The close comparison over the bar is partly fortuitous as the erroneous results during the calm periods contribute to offset a further overprediction of the bar development.

Discussion

Suspended load dominates bed load within the surf zone owing to the low fall velocity (0.013 m/s) of the fine-grain sand (Table 1). This low fall velocity means that the grains remain in suspension much longer, with less turbulent energy required. The sediments within the surf zone were well-sorted fine sand, while those near the shoreline and on the foreshore were coarse and not well sorted. There is very little overlap in sediment size between the two sands. The sediment samples were taken only once on October 15, after the bar was well established. It is conjectured that the fines were winnowed out of the sand near the shoreline and moved offshore, supplying sediment for bar growth. Sampling the sediments on a single day is obviously insufficient to provide much information concerning sediment processes. Future experiments at this site should take advantage of the differences in sediment distributions across shore by sampling on a more frequent basis (at least daily).

In an effort to determine the separate contributions by long waves, short waves, and the mean currents to the model trans-

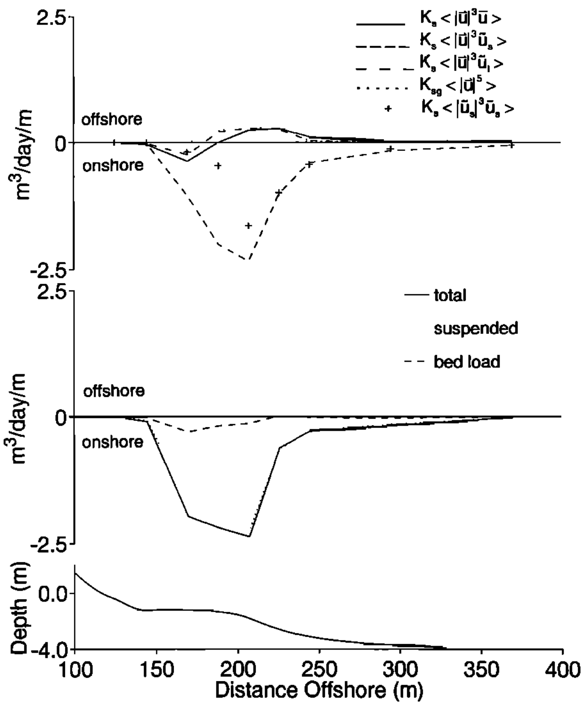

Figure 12. For low swell waves on October 6, 1990, at low tide, (top) cross-shore distributions of 90-min-averaged suspended sediment transport terms $K_s\langle|\mathbf{u}|^3\bar u\rangle$ (solid line), $K_s\langle|\mathbf{u}|^3\tilde u_s\rangle$ (dashed line) and their approximations $K_s\langle|\tilde u_s|^3\tilde u_s\rangle$ (pluses), $K_s\langle|\mathbf{u}|^3\tilde u_l\rangle$ (dash-dotted line) and gravity term $K_{sg}\langle|\mathbf{u}|^5\rangle$ (dotted lines). (middle) The bed load (dashed line), suspended (dotted line), and total (solid line) transports. (bottom) Bottom profile is shown in bottom panel.

port, the terms in (2) are expanded. The bed load is proportional to the product of the velocity modulus (equation (3)) squared with the cross-shore velocities (equation (4)) and is directly expanded,

$$\langle|\mathbf{u}|^2 u\rangle = \langle\tilde u_s^3\rangle + \langle\bar v^2\bar u\rangle + 3\langle\tilde u_s^2\tilde u_l\rangle + 3\langle\tilde u_s^2\bar u\rangle + \cdots \quad (7)$$

where only the three largest of the 18 terms have been retained.

The suspended load terms, however, cannot be directly expanded but can be approximated by series expansions. The suspended loads outside and inside the surf zone are considered separately. Outside the surf zone, where the mean longshore current tends to zero, $\tilde u_s$ is the dominate term, and expanding in a Taylor series [cf. *Bowen*, 1980]

$$\langle|\mathbf{u}|^3 u\rangle \approx \langle|\tilde u_s|^3\tilde u_s\rangle + 4\langle|\tilde u_s|^3\bar u\rangle + 4\langle|\tilde u_s|^3\tilde u_l\rangle + \cdots \quad (8)$$

The first term on the right-hand side of (8) contributes due to the skewness of the short wave velocities, which is negative outside the surf zone, resulting in onshore transport. The second term is associated with the undertow and results in offshore transport. The first term dominates outside the surf zone, where (8) is approximated by

$$\langle|\mathbf{u}|^3 u\rangle \approx \langle|\tilde u_s|^3\tilde u_s\rangle \quad (9)$$

First, a mild wave day is examined on October 6 when the beach was building due to incident long period swell, when many of the current meters were outside the surf zone, and when tidal effects on the sediment transport are most evident. Waves were essentially constant from October 5–7 with periods of 10–12 s, H_{rms} heights of about 0.5 m, and incident wave angles measured in 8 m depth of 26–36°, driving weak longshore currents to the north. To understand the mechanisms causing the sediment transport and the effect of the tide, cross-shore distributions of various sediment transport terms are shown for low and high tide (Figures 12 and 13, top). Figures 12 and 13 (middle) show the bed load, suspended, and total transports. The suspended sediment transport was always an order of magnitude greater than the bed load. The dominant mode is onshore directed suspended transport due to the skewness of the incident short wave velocities, which is reasonably approximated by (9). Only small contributions to the suspended load are apparent due to the long waves or mean undertow. Transport extends farther offshore at low tide, when waves were breaking farther offshore, and is considerably greater. The horizontal short wave velocity described using linear shallow water theory, $\tilde u_s \propto H_{\mathrm{rms}}/\sqrt{h}$, predicts that decreased depth at low tide results in increased velocities for waves of the same height.

During the storm periods, examination of the mean and wave velocities inside the surf zone (Figures 5–9) show the longshore current is the largest term. Assuming inside the surf zone during storm conditions, $\bar v \gg \tilde u_s \sim \bar u \sim \tilde u_l > \tilde v_l \sim \tilde v_s$, the magnitude of the velocity vector is expanded in a binomial series

$$|\mathbf{u}_t|^3 \approx |\bar v|^3 + \tfrac{3}{2}|\bar v|\,|u|^2 + \cdots \quad (10)$$

Substituting into the suspended transport term

$$\begin{aligned}\langle|\mathbf{u}|^3 u\rangle \approx{}& |\bar v|^3\bar u + \tfrac{3}{2}|\bar v|\bar u(\bar u^2 + \langle\tilde u_s^2\rangle + \langle\tilde u_l^2\rangle) + \tfrac{3}{2}|\bar v|(\langle|\tilde u_s|^2\tilde u_s\rangle \\ &+ \langle|\tilde u_l|^2\tilde u_l\rangle) + 3|\bar v\bar u|\bar u(\langle|\tilde u_s|\rangle + \langle|\tilde u_l|\rangle) \\ &+ 3|\bar v\bar u|(\langle|\tilde u_s|\tilde u_s\rangle + \langle|\tilde u_l|\tilde u_l\rangle) + \cdots\end{aligned} \quad (11)$$

where the short and long waves are assumed uncorrelated and

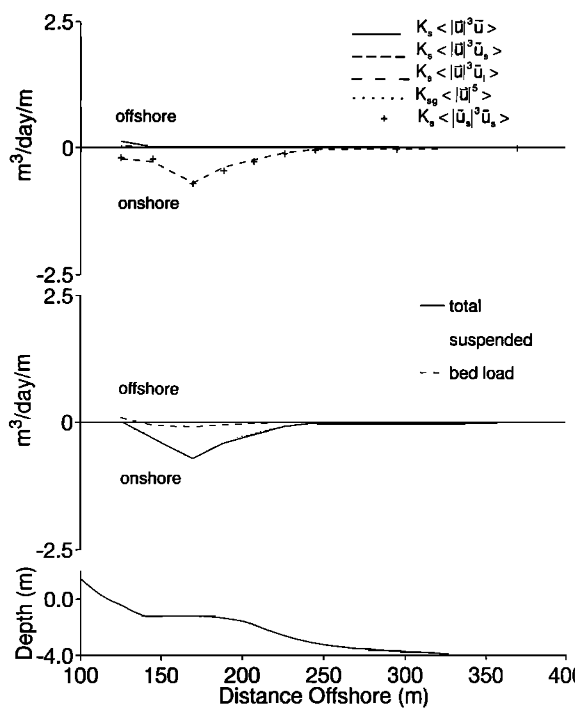

Figure 13. Same as Figure 12, except for low swell waves on October 6, 1990, at high tide.

the corollary that the absolute value of a sum of collinear terms is equal to the sum of absolute values has been applied. The direction of transport of the first two terms is determined by the cross-shore mean current which is offshore within the surf zone due to the undertow. In applying (11), it is found that the last term in brackets is negligible but that other terms can contribute. The lowest-order term only contains mean currents,

$$\langle |\mathbf{u}|^3 u\rangle \approx |\bar{v}|^3 \bar{u} \tag{12}$$

as the lowest-order terms associated with oscillatory terms average to zero.

The cross-shore transport increases greatly during the storms. The transport terms are examined on October 10 at high tide near the beginning of the storms for moderate wave heights with increased longshore currents (Figure 14) and at the height of the storm at low tide on the October 12 (Figure 15). Suspended sediment terms involving $|\mathbf{u}|^3\tilde{u}_s$, $|\mathbf{u}|^3\tilde{u}_l$, $|\mathbf{u}|^3\bar{u}$ and their approximations inside the surf zone for large longshore current (equation (11)) and its lead term $|\bar{v}|^3\bar{u}$ (equation (12)) and outside the surf zone $|\tilde{u}_s|^3\tilde{u}_s$ (equation (9)) are shown in Figures 14 and 15 (top) (note different ordinate scales for each day). The odd moments can transport sediments either onshore or offshore. The even moments transport suspended sediments only onshore. The primary onshore directed term is due to short wave velocity skewness (equation (9)). The odd moments associated with the undertow were always directed offshore.

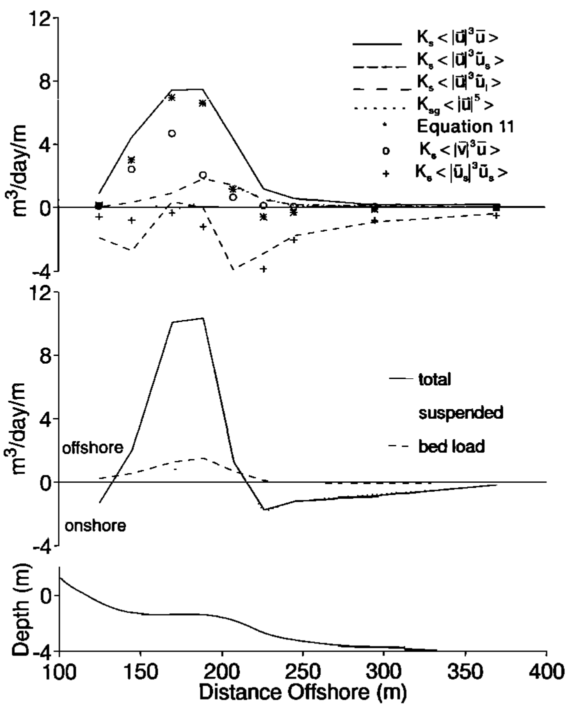

Figure 14. At the beginning of the storm on October 10, 1990, at high tide, (top) cross-shore distributions of 90-min-averaged suspended sediment transport terms $K_s\langle|\mathbf{u}|^3\bar{u}\rangle$ (solid line) and their approximations in the surf zone for large longshore current from (10) (stars) and (11), $K_s|\bar{v}|^3\bar{u}$ (circles), $K_s\langle|\mathbf{u}|^3\tilde{u}_s\rangle$ (dashed line) and their approximations, $K_s\langle|\tilde{u}_s|^3\tilde{u}_s\rangle$ (pluses), $K_s\langle|\mathbf{u}|^3\tilde{u}_l\rangle$ (dash-dotted line) and gravity term $K_{sg}\langle|\mathbf{u}|^5\rangle$ (dotted line). (middle) The bed load (dashed line), suspended (dotted line), and total (solid line) transports.

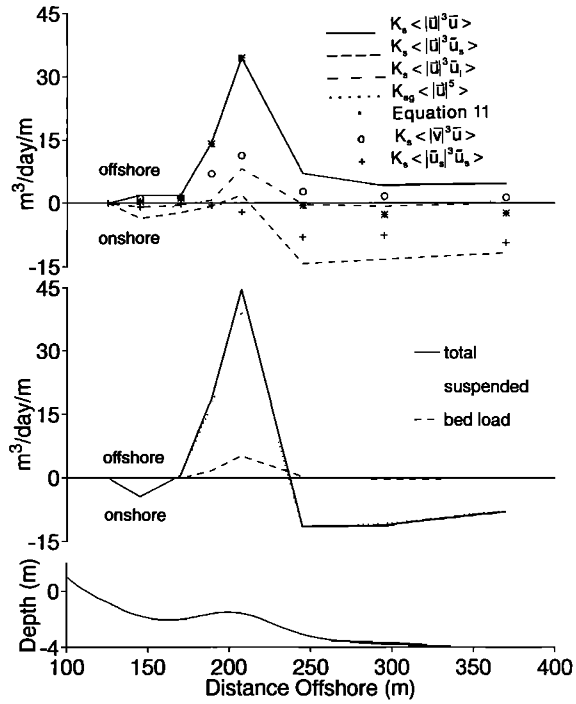

Figure 15. Same as Figure 14, except during the storm on October 12, 1990, at low tide.

Outside the surf zone, the model transport is onshore, primarily due to suspended transport forced by the skewness of the nonlinear waves and opposed by transport offshore due to undertow, with a net onshore transport. *Jaffe et al.* [1984], earlier at Duck, measured suspended sediment flux with current and optical backscatter meters; they found during a time of beach building under moderate waves that the net onshore transport was due to oscillatory short waves, which occurred simultaneous with a weaker offshore transport owing to the undertow throughout the surf zone.

Inside the surf zone, where the maximum longshore current velocity over the trough is almost 1 m/s (see Figure 8), the model-predicted suspended and bedload transport is offshore, primarily due to the longshore current and short waves mobilizing the sediments and the undertow transporting the sediments offshore (that is, suspended sediment transport is well approximated by (11)). About half the transport during the storms with large longshore currents is explained by the longshore current alone mobilizing the sediments with transport offshore by undertow (equation (12)). There was also contribution by long waves, but it was generally smaller in magnitude and directed offshore with a maximum over the bar. The gravity contribution to the suspended sediment transport was similar in magnitude to the long wave contribution and is maximum where the slope is steepest on the backside of the bar and on the foreshore.

During the storm on October 12 (Figure 15) the cross-shore distributions of terms are similar to those described on October 10, with a threefold increase in transport. The maximum longshore current exceeded 1 m/s over the trough and extended much farther offshore due to waves breaking outside the bar (Figure 9). The short wave contribution moved the sediments onshore due to velocity skewness, and mean cross-shore current contribution moved the sediments offshore. The distribution of offshore-directed transport reflects the cross-shore distribution of the undertow, which is greatest over the bar. The net transport is shoreward offshore of the bar and inner trough/foreshore region and is directed offshore over the outer trough/bar region.

Mean velocities within the surf zone during the storm were always above the threshold velocity for suspension of the fine-grained sediments (~0.23 m/s [cf. *Dyer*, 1986], indicated by the horizontal dashed lines in Figures 5–7)) due to the strong longshore current. Since sediments were always predicted to be mobilized, they could be acted on by several different mechanisms to transport them in the cross-shore direction. This process is different than simulations in two-dimensional laboratory studies that have no longshore current.

Long wave transport was calculated using $|\mathbf{u}|^3\tilde{u}_l$. The largest contribution by the long waves would be expected due to phase coupling with the short wave variance. Outside the surf zone and over the bar, phase coupling can exist due to group-bound long waves, which results in positive correlation (in this coordinate system) and thus offshore transport. Near the shoreline the phase coupling would be expected to be negative due to the long waves slowly modulating the depth of breaking of the short wave variance [*Abdelrahman and Thornton*, 1987], resulting in onshore transport. The results suggest the long waves tended to contribute in these manners, with maximum transport offshore over the bar. However, the importance of long waves may not have been fully assessed. For example, the bar generation by *Holman and Bowen* [1982] is based on the long wave mean drift velocity, which in our analysis would be contained in the mean current term and not identified as a long wave contribution. It is also noted that the method of using Fourier filtering to separate oscillatory contributions may also diminish long wave contribution. Long wave skewness would be associated with a set of phase-locked harmonics at higher frequencies, and by filtering high-frequency information, long wave skewness could be diminished. Bispectral analysis would be needed to properly assess the importance of long wave skewness, which is beyond the scope of this paper.

The necessary assumption of alongshore homogeneity to calculate the cross-shore transport was obviously not always valid (see Figure 2). The morphology early in the experiment (October 6–9) was crescentic, three-dimensional bars with approximately 100 m scale. To mitigate this problem, the cross-shore profiles used in the calculations were averaged 200 m up- and downcoast. After the storms started, the bottom contours were approximately straight and parallel (October 10–16), during which the assumption of alongshore homogeneity seems reasonable. It is noted that no rip currents indicating three-dimensional circulation were observed during the period October 6–16. Clearly, using only the cross-shore component of transport may not be sufficient to account for complex bathymetric evolution and may account for some of the observed differences between model and observations early in the experiment.

The calculated divergence of the sediment flux was not well resolved with the current meters ($\Delta x \sim 20$ m). Inspection of the bottom profiles in Figure 3 shows that over the bar and trough the sign of the slope changed at each velocity measurement location. Hence the downslope bed load and suspended load terms in (2) changed sign at each position over the bar and trough. Therefore, in future experiments at this beach, it is recommended that the separation distance between sensors be closer together to better resolve the sediment flux divergence.

The Bowen/Bailard model specifies the velocity at the top of the bottom boundary layer and is evaluated using measured velocities as input. Since the velocity inputs to the model are measured (versus modeled), they represent "near-perfect" velocity input including contributions from mean currents, waves (including surf beat, edge waves, shear instabilities, sea, and swell), and turbulence. The velocities were measured in midwater column (see Figure 3). The short wave velocities were corrected to the bottom using the linear wave theory transfer function, which gives a reasonable approximation [*Guza and Thornton*, 1980]. Since the measured velocities included contributions by both waves and turbulence, the turbulence contribution was also modified (slightly decreased) by the transfer function. Turbulence is generated due to shear in the bottom boundary layer of the waves and currents and at the surface due to wind shear and injection by breaking waves. Using measurements at midwater column transformed to represent turbulence at the top of the bottom boundary layer overestimates turbulence from the surface (therefore transfer function works in correct direction) and underestimates turbulence generated in the bottom boundary layer (transfer function acting in wrong direction). Since short wave velocity intensities are generally an order of magnitude greater than turbulent velocity intensities (i.e., turbulence less than 1% in kinetic energy) within the surf zone [*George et al.*, 1994], it is felt applying a wave transfer function to improve the short wave velocity estimates at the bed is appropriate.

The mean currents in both alongshore and cross-shore have vertical shear and were not depth corrected; therefore midwater column measurements of mean currents can introduce errors in application to the model. The vertical profile of longshore current is approximately logarithmic within the trough region, where the midwater column measurements overestimate velocities at the top of the bottom boundary layer, but are more uniform where the waves break [*Thornton et al.*, 1996]. The vertical profile of the mean cross-shore flow also exhibits considerable vertical shear. Between the crest and trough of the waves the mean cross-shore flow is directed onshore due to mass transport of the waves. In the water column below the crest, the flow is generally offshore due to the undertow forced by the pressure gradient of the wave setup. Thus errors can occur, particularly for current meters high in the water column (as at cm1), where the inferred velocity may have been, at times, in the wrong direction.

The model generally did not behave properly during mild wave conditions, predicting offshore bar migration instead of the measured onshore bar migration. The discrepancy in the model appears to be associated with the short wave asymmetry term underestimating onshore transport over the bar where the waves break and/or the offshore transport by undertow being too strong in this region. When waves break, they tend to become Gaussian and lose their asymmetry. The model predicts reduced transport by the short waves over the bar during mild wave conditions; this behavior in the short wave transport is evident at cm5 (Figures 14 and 15).

Similar behavior was found by *Roelvink and Stive* [1989] in a comparison of the Bowen/Bailard model with laboratory data. They attribute the deficiency to the basic model assumption that the sediments respond instantaneously to the fluid forcing in a quasi-steady manner and are in phase with the fluid stress. This is a sensible assumption in the original formulation by *Bagnold* [1956] applied to unidirectional river flow, but it may not always be a good assumption under oscillatory wave-induced flows, particularly over a rippled bed. Measurements of suspended sediment flux in the field [e.g., *Hanes*, 1990] show the amount of suspended sediments tend to be very episodic (instead of a quasi-steady response), suggesting processes much more nonlinear than formulated in this model. *Roelvink and Stive* [1989] concluded that the lack of prediction of onshore transport just outside the surf zone was due to the rippled bed, resulting in transport that was out of phase with the velocity forcing. Although bed forms were not measured during this experiment, ripples have been observed by the authors throughout the surf zone during mild wave conditions at this location on other occasions.

Comparison of the cumulative measured and predicted profile changes over the 10 days (Figure 11) shows that a bar/trough is predicted, but with the trough underpredicted and the bar displaced slightly offshore. Similar differences between measured and predicted profiles were found in the laboratory by *Roelvink and Stive* [1989, Figure 8]. In an attempt to correct the Bowen/Bailard model they added a stirring mechanism due to breaking waves to enhance the transport. This mechanism is based on modeling the turbulent kinetic energy (TKE) and resulted in some improvement by increasing the amount of predicted change in bathymetry [see *Roelvink and Stive*, 1989, Figure 7], but it did not translate the location of the bar shoreward. Since the model application here is based on measured data, we have not included this enhancement as TKE modeling is beyond the intent of this paper.

Conclusions

The energetics-based sediment transport model by Bowen/Bailard is generally considered the best predictive model presently available. Applying the measured velocities and bathymetry from the DELILAH field experiment provides a test of the model. The calculated suspended transport was approximately an order of magnitude greater than the bed load during the DELILAH experiment due to the low fall velocity of the fine-grain sand within the surf zone. The model predicted the offshore bar movement during the storm periods but underpredicted trough development. The model gave inconsistent predictions of the bar movement during moderate wave conditions when changes were small.

A tidal signature was evident throughout the cross-shore for each mode of flow, suggesting that future experiments should acquire sediment flux data continuously over the tidal cycle and that in predicting bathymetric changes, the integration time step should resolve the tidal cycle. The bar generation mechanism identified by the model during the storm waves was the result of onshore transport outside the surf zone by the short wave velocity skewness converging with sand from within the surf zone, where it is primarily suspended by a strong longshore current and short waves (including turbulence) and transported offshore by an undertow. Inside the surf zone, the mean, short, and long wave velocity components varied both spatially and temporally and were all of the same order within the surf zone. However, the longshore current was the largest component due to incident waves at large angles, and in raising the velocities to high-order moments in the application of the model, the mean longshore current forcing coupled with the undertow (equation (12)) accounted for about half the sediment transport prediction within the surf zone. The longshore current exceeded the threshold velocity for suspended sediments during most of the experiment, keeping the sediment in suspension, as they were acted upon by the offshore-directed undertow. The importance of the mean longshore current during the DELILAH experiment is contrary to the conventional assumption that the short waves cause the primary stress to mobilize and suspend the sediments. It is hypothesized that the linear, alongshore bar formation is associated with strong longshore currents during times of storm waves. Longshore currents are at alongshore wave number equal to zero, corresponding to an infinite alongshore length scale.

The beach did not ever appear to be in equilibrium. During low wave conditions the beach was slowly building, and during storm conditions a bar was being developed. Previous studies by *Lippmann and Holman* [1990] have shown that the morphology at this beach continually changes, going from a linear bar during storms to various three-dimensional formations during other times.

The model gave surprisingly reasonable predictions during storms based on coefficients that were derived for streamflow by *Bagnold* [1956]. It is possible that the good agreement may be, in part, because the strong longshore current present during most of the experiment may have closely resembled streamflow.

Acknowledgments. The data presented here resulted from the cooperative efforts between DELILAH investigators, who provided the cables, calibrations, and deployment resources necessary to conduct a successful surf zone experiment, and, in particular, the FRF staff. The authors are indebted to efforts of the many people who contributed to the data collection and quality control. Much of the computations were performed by M. Bristow, Naval Postgraduate School. The authors thank T. Lippmann for his helpful suggestion and careful editing of the manuscript and the reviewers, whose critical comments improved the manuscript. E.B.T. was funded by ONR Coastal Dynamics grant N00114-94-AF-0002. W.A.B. was supported by the Coastal Research and Development Program of the U.S. Army Corps of Engineers. Permission to publish this paper was granted by the Chief of Engineers.

References

Abdelrahman, S. M., and E. B. Thornton, Changes in the short wave amplitude and wave number due to the presence of infragravity waves, paper presented at Specialty Conference on Coastal Hydrodynamics, Am. Soc. of Civ. Eng., New York, 1987.

Bagnold, R. A., Flow of cohesionless grains in fluids, *Philos. Trans. R. Soc. London*, *249*, 235–297, 1956.

Bagnold, R. A., Mechanics of marine sedimentation, in *The Sea, Idea and Observations*, vol. 3, pp. 507–528, Wiley-Intersci., New York, 1963.

Bagnold, R. A., An approach to the sediment transport problem from general physics, *Geol. Surv. Prof. Pap. 422-I*, U.S. Dep. of the Interior, Washington, D.C., 1966.

Bailard, J. A., An energetics total load sediment transport model for a plane sloping beach, *J. Geophys. Res.*, *86*, 10,938–10,954, 1981.

Battjes, J. A., and J. P. F. M. Janssen, Energy loss and set-up due to breaking in random waves, in *Proceedings of the 16th International Conference on Coastal Engineering*, pp. 569–587, Am. Soc. of Civ. Eng., New York, 1978.

Bowen, A. J., Simple models of nearshore sedimentation; beach profiles and longshore bars; in *The Coastline of Canada*, edited by S. B. McCann, *Pap. Geol. Surv. Can.*, *80-10*, 1–11, 1980.

Carter, T. G., P. L. F. Liu, and C. C. Mei, Mass transport by waves and offshore sand bedforms, *J. Waterw. Harbors Coastal Eng. Div. Am. Soc. Civ. Eng.*, *99*, 165–184, 1973.

Church, J. C., and E. B. Thornton, Effects of breaking wave induced turbulence within a longshore current model, *Coastal Eng.*, *20*, 1–28, 1993.

Dally, W. R., Longshore bar formation–Surf beat or undertow?, in *Proceedings of Coastal Sediments '87*, pp. 71–86, Am. Soc. of Civ. Eng., New York, 1987.

Dally, W. R., and R. G. Dean, Suspended sediment transport and beach profile evolution, *J. Waterw. Port, Coastal Ocean Div. Am. Soc. Civ. Eng., 110*, 15–33, 1984.

Dyer, K. R., *Coastal and Estuarine Sediment Dynamics*, 342 pp., John Wiley, New York, 1986.

Dyhr-Nielsen, M., and T. Sorensen, Sand transport phenomena on coast with bars, in *Proceedings of the 12th International Conference on Coastal Engineering*, pp. 855–866, Am. Soc. Civ. Eng., New York, 1970.

George, R., R. E. Flick, and R. T. Guza, Observation of turbulence in the surf zone, *J. Geophys. Res., 99*, 801–810, 1994.

Greenwood, B., and P. D. Osborne, Equilibrium slopes and cross-shore velocity asymmetries in a storm-dominated, barred nearshore system, *Mar. Geol., 96*, 211–235, 1991.

Guza, R. T., and E. B. Thornton, Local and shoaled comparisons of sea surface elevations, pressures, and velocities, *J. Geophys. Res., 85*, 1524–1530, 1980.

Guza, R. T., and E. B. Thornton, Velocity moments in the nearshore, *J. Waterw. Port Coastal Ocean Div. Am. Soc. Civ Eng., III*, 235–256, 1985a.

Guza, R. T., and E. B. Thornton, Observations of surf beat, *J. Geophys. Res., 90*, 3161–3172, 1985b.

Hanes, D. M., The structure of events of intermittent suspension of sand due to shoaling waves, in *The Sea*, vol. 9, edited by B. LeMehaute and D. M. Hanes, pp. 941–954, Wiley-Intersci., New York, 1990.

Holman, R. A., and A. J. Bowen, Bars, bumps, and holes: Models for the generation of complex beach topography, *J. Geophys. Res., 87*, 457–468, 1982.

Holman, R. A., and A. H. Sallenger Jr., Sand bar generation: A discussion of the Duck Experiment Series, *J. Coastal Res., 15*, 76–92, 1993.

Howd, P. A., A. J. Bowen, and R. A. Holman, Edge waves in the presence of strong longshore currents, *J. Geophys. Res., 97*, 11,357–11,371, 1992.

Jaffe, B. E., R. W. Sternberg, and A. H. Sallenger, The role of suspended sediment in shore normal beach profile changes, in *Proceedings of the 19th International Conference on Coastal Engineering*, pp. 1983–1996, Am. Soc. Civ. Eng., New York, 1984.

Komar, P. D., and C. E. Reimers, Grain shape effects on settling rates, *J. Sediment. Petrol., 45*, 697–703, 1978.

Lippmann, T. L., and R. A. Holman, The spatial and temporal variability of sand bar morphology, *J. Geophys. Res., 95*, 11,575–11,590, 1990.

Oltman-Shay, J., P. A. Howd, and W. A. Birkemeier, Shear instabilities of the mean longshore current, 2, Field data, *J. Geophys. Res., 94*, 18,031–18,042, 1989.

Richmond, B. M., and A. H. Sallenger Jr., Cross-shore transport of bimodal sands, in *Proceedings of the 19th International Conference on Coastal Engineering*, pp. 1997–2007, Am. Soc. Civ. Eng., New York, 1984.

Rienecker, M. M., and J. D. Fenton, A Fourier approximation method for steady water waves, *J. Fluid Mech., 104*, 119–137, 1981.

Roelvink, J. A., Surf beat and its effect on cross-shore profiles, Ph.D. dissertation, 150 pp., Technical Univ., Delft, Netherlands, 1993.

Roelvink, J. A., and M. J. F. Stive, Bar generating cross-shore flow mechanisms on a beach, *J. Geophys. Res., 94*(C4), 4785–4800, 1989.

Stive, M. J. F., A model for cross-shore sediment transport, in *Proceedings of the 20th International Conference on Coastal Engineering*, pp. 1550–1564, Am. Soc. Civ. Eng., New York, 1986.

Stive, M. J. F., and J. A. Battjes, A model for offshore sediment transport, in *Proceedings of the 19th International Conference on Coastal Engineering*, pp. 1420–1436, Am. Soc. Civ. Eng., New York, 1984.

Thornton, E. B., and C. S. Kim, Longshore current and wave height modulation at tidal frequency inside the surf zone, *J. Geophys. Res., 98*, 16,509–16,519, 1993.

Thornton, E. B., C. Soares, and T. P. Stanton, Vertical profiles of mean longshore currents and bed shear stresses, in *Proceedings of Coastal Dynamics '95*, Am. Soc. Civ. Eng., New York, in press, 1996.

W. Birkemeier, Field Research Facility, U.S. Army Corps of Engineers, Kitty Hawk, NC 27949.

R. T. Humiston, Naval Pacific Meteorology and Oceanography Center, Box 113, Pearl Harbor, HI 96860.

E. B. Thornton, Oceanography Department, Naval Postgraduate School, Monterey, CA 93943. (e-mail: thornton@hope.oc.nps.navy.mil)

(Received February 16, 1994; revised November 7, 1995; accepted November 17, 1995.)